Controlling spin relaxation with a cavity

A. Bienfait[1], J.J. Pla[2], Y. Kubo[1], X. Zhou[1,3], M. Stern[1,4], C.C. Lo[2], C.D. Weis[5], T. Schenkel[5], D. Vion[1], D. Esteve[1], J.J.L. Morton[2], and P. Bertet[1]

[1]*Quantronics group, Service de Physique de l'Etat Condensé,*

DSM/IRAMIS/SPEC, CNRS UMR 3680,

CEA-Saclay, 91191 Gif-sur-Yvette cedex, France

[2] *London Centre for Nanotechnology, University College London,*

London WC1H 0AH, United Kingdom

[3]*Institute of Electronics Microelectronics and Nanotechnology,*

CNRS UMR 8520, ISEN Department, Avenue Poincaré,

CS 60069, 59652 Villeneuve d'Ascq Cedex, France

[4] *Quantum Nanoelectronics Laboratory, BINA,*

Bar Ilan University, Ramat Gan, Israel and

[5]*Accelerator Technology and Applied Physics Division,*

Lawrence Berkeley National Laboratory, Berkeley, California 94720, USA

(Dated: December 9, 2015)

Abstract

Spontaneous emission of radiation is one of the fundamental mechanisms by which an excited quantum system returns to equilibrium. For spins, however, spontaneous emission is generally negligible compared to other non-radiative relaxation processes because of the weak coupling between the magnetic dipole and the electromagnetic field. In 1946, Purcell realised [1] that the spontaneous emission rate can be strongly enhanced by placing the quantum system in a resonant cavity — an effect which has since been used extensively to control the lifetime of atoms and semiconducting heterostructures coupled to microwave [2] or optical [3, 4] cavities, underpinning single-photon sources [5]. Here we report the application of these ideas to spins in solids. By coupling donor spins in silicon to a superconducting microwave cavity of high quality factor and small mode volume, we reach the regime where spontaneous emission constitutes the dominant spin relaxation mechanism. The relaxation rate is increased by three orders of magnitude when the spins are tuned to the cavity resonance, showing that energy relaxation can be engineered and controlled on-demand. Our results provide a novel and general way to initialise spin systems into their ground state, with applications in magnetic resonance and quantum information processing [6]. They also demonstrate that, contrary to popular belief, the coupling between the magnetic dipole of a spin and the electromagnetic field can be enhanced up to the point where quantum fluctuations have a dramatic effect on the spin dynamics; as such our work represents an important step towards the coherent magnetic coupling of individual spins to microwave photons.

Spin relaxation is the process by which a spin reaches thermal equilibrium by exchanging an energy quantum $\hbar\omega_{\rm s}$ with its environment ($\omega_{\rm s}$ being its resonance frequency) for example in the form of a photon or a phonon, as shown in Fig. 1a. Understanding and controlling spin relaxation is of essential importance in applications such as spintronics [7] and quantum information processing [8] as well as magnetic resonance spectroscopy and imaging [9]. For such applications, the spin relaxation time T_1 must be sufficiently long to permit coherent spin manipulation; however, if T_1 is too long it becomes a major bottleneck which limits the repetition rate of an experiment, and in turn impacts factors such as the achievable sensitivity. Certain types of spins can be actively reset in their ground state by optical [10] or electrical [11] means due to their specific energy level scheme, while methods such as chemical doping have been employed to influence spin relaxation times ex-situ [12]. Nevertheless, an efficient, general and tuneable initialization method for spin systems is still currently lacking.

At first inspection, spontaneous emission would appear an unlikely candidate to influence spin relaxation: for example, an electron spin in free space and at a typical frequency of $\omega_s/2\pi \simeq 8\,{\rm GHz}$, spontaneously emits a photon at a rate of $\sim 10^{-12}\,{\rm s}^{-1}$. However, the Purcell effect provides a means to dramatically enhance spontaneous emission, and thus gain precise and versatile control over spin relaxation [1]. Consider a spin embedded in a microwave cavity of quality factor Q and frequency ω_0.

If the cavity damping rate $\kappa = \omega_0/Q$ is greater than the spin-cavity coupling g, the cavity then provides an additional channel for spontaneous emission of microwave photons, governed by a so-called Purcell rate [6, 13]

$$\Gamma_{\rm P} = \kappa \frac{g^2}{\kappa^2/4 + \delta^2},\tag{1}$$

where $\delta = \omega_0 - \omega_{\rm s}$ is the spin-cavity detuning (see Fig. 1a and Methods).

This cavity-enhanced spontaneous emission can be much larger than in free space, and is strongest when the spins and cavity are on-resonance ($\delta = 0$), where $\Gamma_{\rm P} = 4g^2/\kappa$. Furthermore, the Purcell rate can be modulated by changing the coupling constant or the detuning, allowing spin relaxation to be tuned on-demand. The Purcell effect was used to detect spontaneous emission of radiofrequency radiation from nuclear spins coupled to a resonant circuit [14], but even then the corresponding Purcell rate $\Gamma_{\rm P} \simeq 10^{-16}$ s^{-1} (or 1 photon emitted every 300 million years) was negligible compared to the intrinsic spin-lattice relaxation processes. In order for photon emission to become the dominant spin relaxation mechanism,

both a large spin-cavity coupling and a low cavity damping rate are needed: in our experiment, this is achieved by combining the microwave confinement provided by a micron-scale resonator with the high quality factors enabled by the use of superconducting circuits.

The device consists of two planar aluminium lumped-element superconducting resonators patterned onto a silicon chip which was purified in nuclear-spin-free ^{28}Si and implanted with bismuth atoms (see Fig. 1b) at a sufficiently low concentration for collective radiation effects to be absent. A static magnetic field $\mathbf{B_0}$ is applied in the plane of the aluminium resonators, at an angle θ from the resonator inductive wire, tunable in-situ. The device is mounted inside a copper box and cooled to 20 mK. Each resonator can be used to perform inductive detection of the electron-spin resonance (ESR) signal of the bismuth donors: microwave pulses at ω_0 are applied at the resonator input, generating an oscillating magnetic field B_1 around the inductive wire which drives the surrounding spins; the quantum fluctuations of this field, present even when no microwave is applied, are responsible for the Purcell spontaneous emission. Hahn echo pulse sequences [15] are used, resulting in the emission of a spin-echo in the detection waveguide, which is amplified with a sensitivity reaching the quantum limit thanks to the use of a Josephson Parametric Amplifier [16] and demodulated, yielding the integrated echo signal quadrature A_Q (see Methods). A more detailed setup description can be found in [17].

Bismuth is a donor in silicon [18] with a nuclear spin $I = 9/2$. At cryogenic temperatures it can bind an electron (with spin $S = 1/2$) in addition to those shared with the surrounding Si lattice. The large hyperfine interaction $A\mathbf{S} \cdot \mathbf{I}$ between the electron and nuclear spin, where $\mathbf{S}$ and $\mathbf{I}$ are the electron and nuclear spin operators and $A/h = 1475$ MHz, produces a splitting of 7.375 GHz between the ground and excited multiplets at zero magnetic field (see Fig. 1d for the complete energy diagram [19]). This makes the system ideal for coupling to superconducting circuits [20, 21]. At low fields ($B_0 < 10\,\mathrm{mT}$, compatible with the critical field of aluminium) all $\Delta m_\mathrm{F} = \pm 1$ transitions are allowed, m_F being the projection of the total spin ($\mathbf{F} = \mathbf{I} + \mathbf{S}$) along B_0. Considering only the transitions with largest matrix element, resonator A ($\omega_{0A}/2\pi = 7.245$ GHz, $Q_A = 3.2 \times 10^5$) crosses the $|F, m_F\rangle = |4, -4\rangle \leftrightarrow |5, -5\rangle$ transition, whilst resonator B ($\omega_{0B}/2\pi = 7.305$ GHz, $Q_B = 1.1 \times 10^5$) crosses the transitions $|4, -4\rangle \leftrightarrow |5, -5\rangle$, $|4, -3\rangle \leftrightarrow |5, -4\rangle$, and $|4, -2\rangle \leftrightarrow |5, -3\rangle$ (see Figs. 2a and b).

The echo signal A_Q from each resonator as a function of B_0 shows resonances at the expected magnetic fields, split into two peaks of full-width-half-maximum $\Delta\omega/2\pi \sim 2$ MHz

(see Fig. 2a). As explained in [17], this splitting is believed to be the result of strain induced in the silicon by the aluminium surface structure, which is non-negligible at the donor implant depth of ~ 100 nm. In the following we focus on the lower-frequency peak of the $|4, -4\rangle \leftrightarrow |5, -5\rangle$ line which corresponds to spins lying under the wire. Over the region occupied by these spins, the B_1 field amplitude varies by less than $\pm 2\%$, as evidenced by the well-defined Rabi oscillations observed when we sweep the power of the refocusing pulse P_{in} at the cavity input (see Fig. 2c), allowing us to determine the input power of a π pulse for a given pulse duration.

We measure the relaxation time T_1 by performing an "inversion-recovery" experiment [22] (see schematic, top of Fig. 2a), with the static field B_0 aligned along x ($\theta = 0$). A π pulse first inverts the spins whose frequency lies within the resonator bandwidth $\kappa_A/2\pi = 23$ kHz (or $\kappa_B/2\pi = 68$ kHz); note that this constitutes a small subset of the total number of spins since $\kappa_{A,B} \ll \Delta\omega$. After a varying delay T, a Hahn echo sequence provides a measure of the longitudinal spin polarization. Fitting the data with decaying exponentials, we extract $T_1 = 0.35$ s for resonator A and $T_1 = 1.0$ s for resonator B.

For a quantitative comparison with the expected Purcell rate, it is necessary to evaluate the spin-resonator coupling constant $g = \gamma_e \langle F, m_F | S_x | F+1, m_F - 1 \rangle \, \|\delta \mathbf{B}_\perp\|$, where $\gamma_e/2\pi \simeq 28$ GHz/T is the electronic gyromagnetic ratio and $\delta \mathbf{B}_\perp$ is the component of the resonator field vacuum fluctuations orthogonal to $\mathbf{B_0}$ (see Methods). A numerical estimate yields $g_0/2\pi = 56 \pm 1$ Hz for the spins located below the resonator inductive wire that are probed in our measurements and for $\theta = 0$. An independent estimate is obtained by measuring Rabi oscillations. Their frequency $\Omega_R = 2g_0\sqrt{\bar{n}}$ directly yields g_0 upon knowledge of the average intra-cavity photon number $\bar{n}$, which can be determined with a $\sim 30\%$ imprecision from P_{in} and the measured resonator coupling to the input and output antennae (see Methods). We obtain $g_0/2\pi = 50 \pm 7$ Hz for resonator A and 58 ± 7 Hz for resonator B, compatible with the numerical estimate. The corresponding resonant Purcell spontaneous emission time is $\Gamma_P^{-1} = 0.36 \pm 0.09$ s for resonator A and 0.81 ± 0.17 s for resonator B, in agreement with the experimental values.

According to Eq. 1, a Purcell-limited T_1 should be strongly dependent on the spin-cavity detuning. We introduce a magnetic field pulse of duration T between the spin excitation and the spin-echo sequence (see Fig. 3a), which results in a temporary detuning δ of the spins. The echo signal amplitude A_Q as a function of T yields their energy relaxation time

while they are detuned by δ. To minimize the influence of spin diffusion [22], the spin excitation is performed here by a high-power long-duration saturating pulse (see Fig. 3a and Methods) instead of an inversion pulse as in Fig. 2d. As evident in Fig. 3b, we find that the decay of the echo signal is well fit by a single exponential with a decay time increasing with $|\delta|$. The extracted $T_1(\delta)$ curve (see Fig. 3c) shows a remarkable increase of T_1 by up to 3 orders of magnitude when the spins are detuned away from resonance, until it becomes limited by a non-radiative energy decay mechanism with rate $\Gamma_{\mathrm{NR}}^{-1} = 1600 \pm 300\,\mathrm{s}$. Given the doping concentration in our sample, this rate is consistent with earlier measurements of donor spin relaxation times [23], which have been attributed to charge hopping, but could also arise here from spatial diffusion of the spin magnetisation away from the resonator mode volume. Figure 3c shows that the $T_1(\delta)$ measurements are in agreement with the expected dependence $(\Gamma_{\mathrm{P}}(\delta) + \Gamma_{\mathrm{NR}})^{-1}$, with the only free parameter in this fit being Γ_{NR}.

Having demonstrated the effect of cavity linewidth and detuning on the Purcell rate, we finally explore the effect of modulating the spin-cavity coupling constant g. This can be achieved by varying the orientation θ of the static magnetic field B_0 in the x-y plane (Fig. 1b), adjusting the component of the microwave magnetic field (mostly along y under the inductive wire) which is orthogonal to B_0. More precisely, $g(\theta) = \gamma_{\mathrm{e}} \langle F, m_F | S_x | F + 1, m_F - 1 \rangle \sqrt{\delta B_{1y}^2 \cos(\theta)^2 + \delta B_{1z}^2}$ (noting that $\delta B_{1x} = 0$), and we expect $\delta B_{1z} \ll \delta B_{1y}$ for the spins lying under the wire that are probed in these measurements. This is verified experimentally by measuring the Rabi frequency as a function of θ, as shown in Fig. 4a & b, allowing us to extract $g(0)/2\pi = 58\,\mathrm{Hz}$ and $g(\pi/2)/2\pi = 17\,\mathrm{Hz}$. As expected, we measure longer spin relaxation times for increasing values of θ, as shown in Fig. 4c, with the relaxation rate T_1^{-1} scaling as $g^2(\theta)$, in agreement with Eq. 1. Overall, the data of Figs. 3 and 4 demonstrate unambiguously that cavity-enhanced spontaneous emission is by far the dominant spin relaxation channel when the spins are resonant with the cavity, since the probability for a spin-flip to occur due to emission of a microwave photon in the cavity is $1/[1 + \Gamma_{\mathrm{NR}}/\Gamma_{\mathrm{P}}(\delta = 0)] = 0.999$, very close to unity.

At this point it is interesting to reflect on the important fact that the spontaneous emission evidenced here is an energy relaxation mechanism which does not require the presence of a macroscopic magnetization to be effective. Under the Purcell effect, each spin independently relaxes towards thermal equilibrium by microwave photon emission, so that when no intra-cavity thermal field is present the sample ends up in a fully polarized state after a time

6

longer than Γ_{P}^{-1}, regardless of its initial state. This is in stark contrast with the well-known phenomenon of radiative damping [24] of a transverse magnetization generated by earlier microwave pulses, which is a coherent collective effect under which the degree of polarization of a sample cannot increase. We also note that had our device possessed a larger spin concentration, spontaneous relaxation would have occurred collectively, manifesting itself as a non-exponential decay of the echo signal on a time scale faster than Γ_P^{-1} [13] and leading to an incomplete thermalization [6, 25]. Such superradiant or maser emission [26] requires the dimensionless parameter $C = Ng^2/(\kappa\Delta\omega)$ called cooperativity (N being the total number of spins) to satisfy $C \gg 1$ [6, 25, 27], which is not the case here because of the large inhomogeneous broadening of the spin resonance caused by strain.

Our demonstrated ability to modulate spin relaxation through 3 orders of magnitude by changing the applied field by less than 0.1 mT opens up new perspectives for spin-based quantum information processing: long intrinsic relaxation times which are desirable to maximise the spin coherence time can be combined with fast, on-demand initialisation of the spin state. Similarly, performing electron spin resonance at dilution refrigerator temperatures can be prohibitively slow without the ability to accelerate spin relaxation on demand. We also anticipate Purcell relaxation will offer a powerful approach to dynamical nuclear polarisation [28, 29], for example by tuning the cavity to match an electron-nuclear spin flip-flop transition, enhancing the rate of cross-relaxation to pump polarisation into the desired nuclear spin state [30] (see Methods). The Purcell rate we obtain could be increased by reducing the transverse dimensions of the inductor wire to yield larger coupling constants, up to $5 - 10 \, \mathrm{kHz}$, bringing the spontaneous emission time below $1 \, \mathrm{ms}$ (enabling faster repetition rates, as well as a higher sensitivity [17]), and opening up the possibility of high-cooperativity coupling of a single spin to the microwave cavity field. Finally, our measurements constitute the first evidence that vacuum fluctuations of the microwave field can affect the dynamics of spins, and are thus a step towards the application of circuit quantum electrodynamics concepts to individual spins in solids.

---

[1] E. M. Purcell, "Spontaneous emission probabilities at radio frequencies," Phys. Rev. **69**, 681 (1946).

[2] P. Goy, J. M. Raimond, M. Gross, and S. Haroche, "Observation of cavity-enhanced single-atom spontaneous emission," Phys. Rev. Lett. **50**, 1903–1906 (1983).

[3] D. J. Heinzen, J. J. Childs, J. E. Thomas, and M. S. Feld, "Enhanced and inhibited visible spontaneous emission by atoms in a confocal resonator," Phys. Rev. Lett. **58**, 1320–1323 (1987).

[4] Y. Yamamoto, S. Machida, Y. Horikoshi, K. Igeta, and G. Bjork, "Enhanced and inhibited spontaneous emission of free excitons in GaAs quantum wells in a microcavity," Optics Communications **80**, 337 – 342 (1991).

[5] J. M. Gérard, B. Sermage, B. Gayral, B. Legrand, E. Costard, and V. Thierry-Mieg, "Enhanced spontaneous emission by quantum boxes in a monolithic optical microcavity," Phys. Rev. Lett. **81**, 1110–1113 (1998).

[6] M. C. Butler and D. P. Weitekamp, "Polarization of nuclear spins by a cold nanoscale resonator," Phys. Rev. A **84**, 063407 (2011).

[7] J. Sinova and I. Žutić, "New moves of the spintronics tango," Nature Materials **11**, 368–371 (2012).

[8] T. D. Ladd, F. Jelezko, R. Laflamme, Y. Nakamura, C. Monroe, and J. L. OBrien, "Quantum computers," Nature **464**, 45–53 (2010).

[9] M. H. Levitt, *Spin dynamics: basics of nuclear magnetic resonance* (John Wiley and Sons, 2001).

[10] L. Robledo, L. Childress, H. Bernien, B. Hensen, P.F.A. Alkemade, and R. Hanson, "High-fidelity projective read-out of a solid-state spin quantum register," Nature **477**, 574 (2011).

[11] J. J. Pla, K. Y. Tan, J. P. Dehollain, W. H. Lim, J. J. L. Morton, D. N. Jamieson, A. S. Dzurak, and A. Morello, "A single-atom electron spin qubit in silicon," Nature **489**, 541–545 (2012).

[12] M. G. Shapiro, G. G. Westmeyer, P. A. Romero, J. O. Szablowski, B. Küster, A. Shah, C. R. Otey, R. Langer, F. H. Arnold, and A. Jasanoff, "Directed evolution of a magnetic resonance imaging contrast agent for noninvasive imaging of dopamine," Nature Biotechnology **28**, 264–270 (2010).

[13] C. J. Wood, T. W. Borneman, and D. G. Cory, "Cavity cooling of an ensemble spin system," Phys. Rev. Lett. **112**, 050501 (2014).

[14] T. Sleator, E. L. Hahn, C. Hilbert, and J. Clarke, "Nuclear-spin noise," Phys. Rev. Lett. **55**,

1742–1745 (1985).

[15] E. Hahn, "Spin echoes," Physical Review **80**, 580–594 (1950).

[16] X. Zhou, V. Schmitt, P. Bertet, D. Vion, W. Wustmann, V. Shumeiko, and D. Esteve, "High-gain weakly nonlinear flux-modulated Josephson parametric amplifier using a SQUID array," Phys. Rev. B **89**, 214517 (2014).

[17] A. Bienfait, J. J. Pla, Y. Kubo, M. Stern, X. Zhou, C.-C. Lo, C. D. Weis, T. Schenkel, M. L. W. Thewalt, D. Vion, D. Esteve, B. Julsgaard, K. Moelmer, J. J. L. Morton, and P. Bertet, "Reaching the quantum limit of sensitivity in electron spin resonance," arXiv:1507.06831 (2015).

[18] G. Feher, "Electron spin resonance experiments on donors in silicon. i. Electronic structure of donors by the electron nuclear double resonance technique," Phys. Rev. **114**, 1219–1244 (1959).

[19] Gary Wolfowicz, Stephanie Simmons, Alexei M. Tyryshkin, Richard E. George, Helge Riemann, Nikolai V. Abrosimov, Peter Becker, Hans-Joachim Pohl, Stephen A. Lyon, Mike L. W. Thewalt, and John J. L. Morton, "Decoherence mechanisms of ^{209}Bi donor electron spins in isotopically pure ^{28}Si," Phys. Rev. B **86**, 245301 (2012).

[20] Gavin W Morley, Marc Warner, A Marshall Stoneham, P Thornton Greenland, Johan van Tol, Christopher WM Kay, and Gabriel Aeppli, "The initialization and manipulation of quantum information stored in silicon by bismuth dopants," Nature materials **9**, 725–729 (2010).

[21] R. E. George, W. Witzel, H. Riemann, N. V. Abrosimov, N. Nötzel, M. L. W. Thewalt, and J. J. L. Morton, "Electron spin coherence and electron nuclear double resonance of Bi donors in natural Si," Phys. Rev. Lett. **105**, 067601 (2010).

[22] A. Schweiger and G. Jeschke, *Principles of pulse electron paramagnetic resonance* (Oxford University Press, 2001).

[23] G. Feher and E. A. Gere, "Electron spin resonance experiments on donors in silicon. ii. Electron spin relaxation effects," Phys. Rev. **114**, 1245–1256 (1959).

[24] N. Bloembergen and R. V. Pound, "Radiation damping in magnetic resonance experiments," Phys. Rev. **95**, 8–12 (1954).

[25] C. J. Wood and D. G. Cory, "Cavity cooling to the ground state of an ensemble quantum system," arXiv:1506.03007 (2015).

[26] G. Feher, J. P. Gordon, E. Buehler, E. A. Gere, and C. D. Thurmond, "Spontaneous emission

of radiation from an electron spin system," Phys. Rev. **109**, 221–222 (1958).

[27] V. V. Temnov and U. Woggon, "Superradiance and subradiance in an inhomogeneously broadened ensemble of two-level systems coupled to a low-Q cavity," Phys. Rev. Lett. **95**, 243602 (2005).

[28] T. R. Carver and C. P. Slichter, "Polarization of nuclear spins in metals," Phys. Rev. **92**, 212–213 (1953).

[29] A. Abragam and M. Goldman, "Principles of dynamic nuclear polarisation," Reports on Progress in Physics **41**, 395–467 (1978).

[30] N. Bloembergen, S. Shapiro, P. S. Pershan, and J. O. Artman, "Cross-relaxation in spin systems," Phys. Rev. **114**, 445–459 (1959)

.

Author contributions A.B., J.J.P., J.J.L.M. and P.B. designed the experiment. X.Z. and D.V. designed and fabricated the Josephson Parametric Amplifier. C.C.L., C.D.W., T.S. provided the bismuth-implanted isotopically purified silicon sample. A.B., J.J.P., and Y.K. fabricated the sample and performed the measurements. A.B., J.J.P., Y.K., J.J.L.M., and P.B. analyzed the data. J.J.L.M., D.E., D.V., and P.B. supervised the project. A.B., J.J.P., Y.K., M.S., D.V., D.E., J.J.L.M. and P.B. all contributed to the writing of the paper.

Additional information Reprints and permission information is available online at http://npg.nature.com/reprintsandpermissions/. Correspondence and requests for materials should be addressed to P.B.

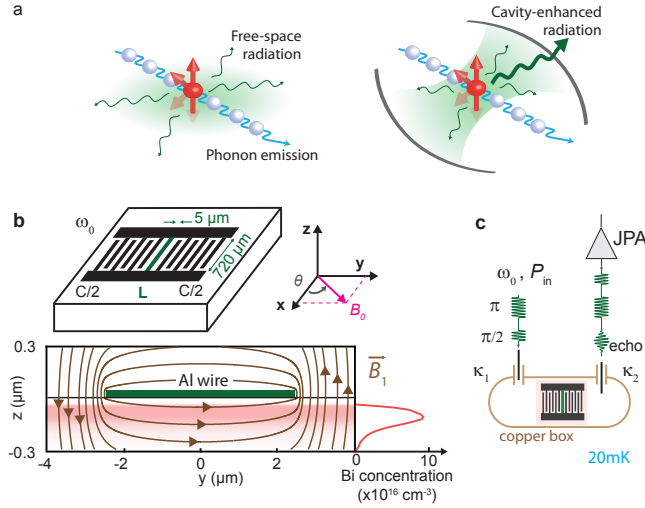**Competing financial interests** The authors declare no competing financial interests.

FIG. 1. **Purcell-enhanced spin relaxation and experimental setup. a)** By placing a spin in a resonant cavity, radiative spin relaxation can be made to dominate over intrinsic processes such as phonon-induced relaxation. **b)** (top) A planar superconducting resonator comprising an interdigitated capacitor in parallel with an inductive wire is fabricated on top of Bi-doped ^{28}Si. A static magnetic field B_0 is applied parallel to the $(x\text{-}y)$ plane of the 50 nm thick aluminium layer with a tunable orientation given by θ. (bottom) Magnetic field lines of the microwave excitation field $\vec{B_1}$ generated by the aluminium wire (arrows) are superimposed over the local concentration of Bi donors (red), obtained by secondary ion mass spectrometry (SIMS). **c)** The sample is mounted in a copper box thermally anchored at 20 mK and probed by microwave pulses via asymmetric antennae coupled with rate $\kappa_1 \approx \kappa_2/5$ to the resonator. Microwave pulses at ω_0 of power P_{in} are sent by antenna 1, and the microwave signal leaving via antenna 2 is directed to the input of a Josephson Parametric Amplifier (JPA).
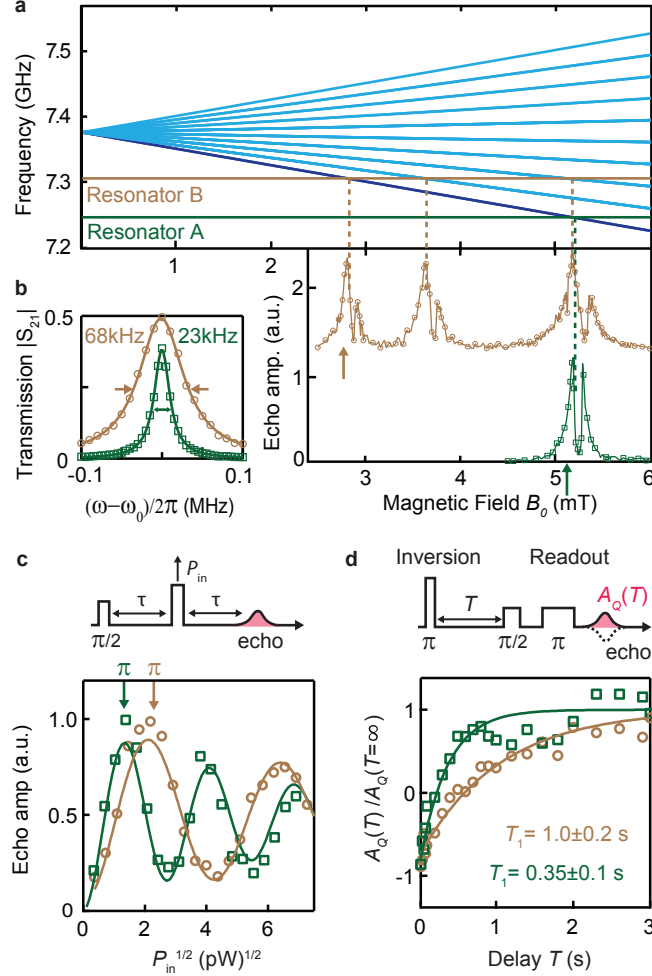
FIG. 2. **ESR spectroscopy and Purcell-limited T_1 measurement. a)** (top) Dominant electron spin resonance transitions of the Si:^{209}Bi spin system (see Methods). We employ two resonators, A (green) and B (yellow), with frequencies 7.246 and 7.305 GHz, which cross up to three spin transitions in the magnetic field range $0 - 6$ mT, as seen in the echo-detected magnetic field sweep (bottom panel, vertically offset for clarity). Subsequent spin relaxation measurements were made at the magnetic fields indicated by the arrows, corresponding to the $|F, m_F\rangle = |4, -4\rangle \leftrightarrow |5, -5\rangle$ transition for each resonator. The doublet structure of each transition is caused by strain exerted by the aluminum film on the donors [17]. **b)** Cavity linewidths for resonators A and B are measured to be 23 and 68 kHz respectively. **c)** Rabi oscillations are driven by varying the cavity input power of the refocusing 5-µs-long π pulse. **d)** The inversion-recovery sequence is used to measure the spin relaxation time T_1. Spin polarisation is measured with a Hahn echo sequence. Rescaled by its value for $T \gg T_1$, A_Q goes from -1 when the spins are fully inverted to $+1$ at thermal equilibrium. (see Methods for full sequence description). Data in this figure were obtained with the static field B_0 parallel to the inductor ($\theta = 0$).
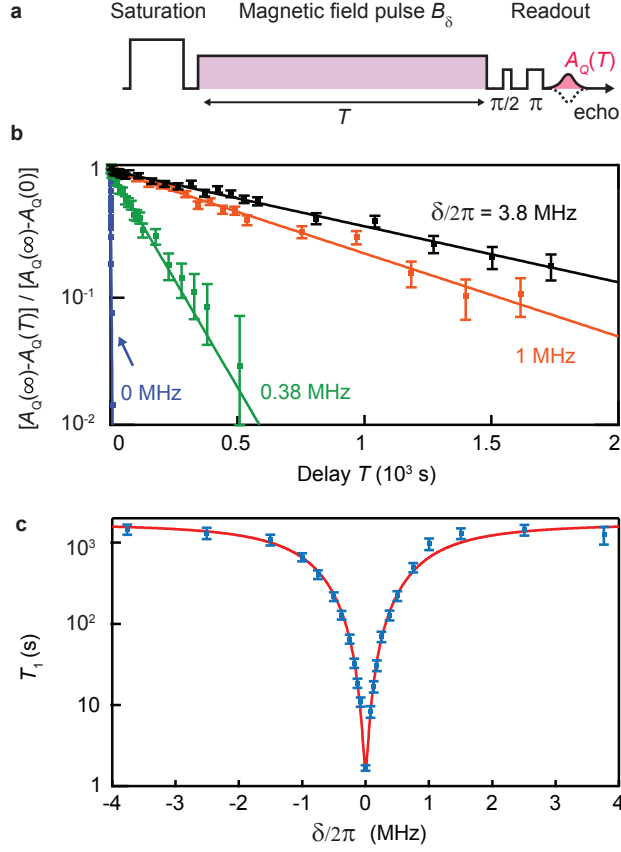
13

FIG. 3.   **Controlling Purcell relaxation by spin-cavity detuning.**   **a)** In-between their saturation and subsequent readout, the spins are detuned from the cavity by $\delta = \frac{d\omega_s}{dB} B_\delta$ by applying a magnetic field pulse of amplitude B_δ, with $\frac{1}{2\pi} \frac{d\omega_s}{dB} \simeq 25$ GHz/T for this transition and magnetic field. **b)** Measured spin polarisation decays (dots) for four different detunings, well fit (lines) to exponential decays, with relaxation time constants T_1 increasing with the detuning (Error bars: single-shot standard deviation (s.d.), n=2001). **c)** Measured T_1 as a function of detuning δ, error bars are fit s.d. estimates. Line is a fit with $(\Gamma_P(\delta) + \Gamma_{NR})^{-1}$, yielding $\Gamma_{NR}^{-1} = 1600$ s. Note that these measurements are taken using resonator B and with $\theta = \pi/4$, which results in $T_1 = 1.7$ s at $\delta = 0$.
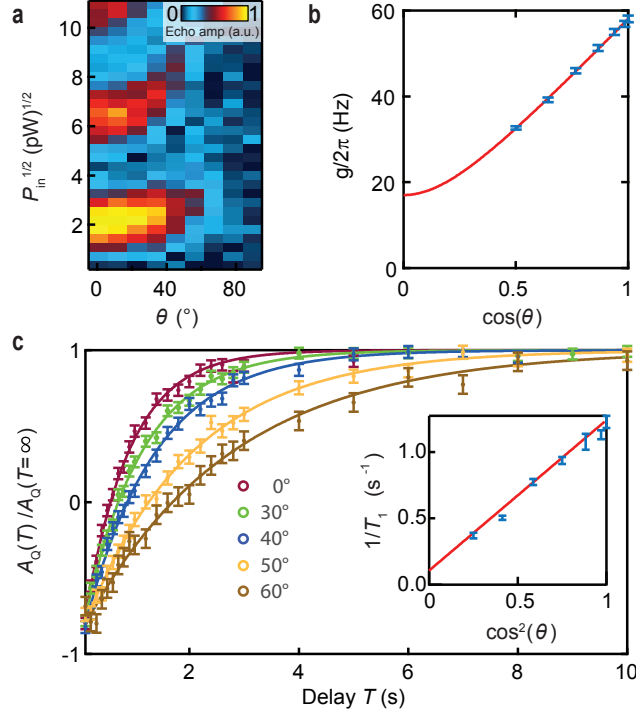
14

FIG. 4. **Dependence of Purcell relaxation on spin-cavity coupling** g. **a)** Rabi oscillations (as in Fig. 2c) measured as a function of field orientation θ (see Fig.1b) are used to extract **b)** the spin-cavity coupling strength g (Error bars are determined by the 30% accuracy on P_{in}). Its dependence on θ is fit to the expression in the main text (red line); the non-zero value of $g(\pi/2)$ is due to the finite out-of-plane component of the microwave magnetic field. **c)** Inversion-recovery measurements (Error bars: single-shot s.d., n=201) as a function of θ confirm that the relaxation time T_1 (see inset) varies as $g(\theta)^2$ (Error bars are fit s.d. estimates). Solid line is the Purcell formula prediction using the $g(\theta)$ dependence fitted from (b). All data in the figure were taken using resonator B.

METHODS

Bismuth donors in silicon Bismuth donors in silicon have the following isotropic spin Hamiltonian[31]: $\hat{H}/h = \mathbf{B} \cdot (\gamma_e \mathbf{S} \otimes \mathbb{1} - \gamma_n \mathbb{1} \otimes \mathbf{I}) + A\,\mathbf{S} \cdot \mathbf{I}$ where the electronic gyromagnetic ratio $\gamma_e/2\pi = 27.997$ GHz/T, the nuclear gyromagnetic ratio $\gamma_n/2\pi = 6.9$ MHz/T and the hyperfine coupling constant $A/h = 1.475$ GHz. For a weak static field B_0 ($B_0 \lesssim 50\,\text{mT}$) oriented along $\mathbf{x}$, the eigenstates of the total angular momentum $\mathbf{F} = \mathbf{S} + \mathbf{I}$ and its projection m_F along B_0 represent good quantum numbers for the 20 electro-nuclear energy states of the Bi:Si system. These eigenstates can be grouped in an $F = 4$ ground and an $F = 5$ excited multiplet separated by a frequency of $(I + 1/2)A/h = 7.35\,\text{GHz}$ in zero-field (see Fig. 1d). Transitions between states verifying $\Delta F \Delta m_F = \pm 1$ can be excited with a field orientated along $\mathbf{y}$ (or $\mathbf{z}$) since their associated matrix element $\langle F, m_F | S_y | F + 1, m_F \pm 1 \rangle = \langle F, m_F | S_z | F + 1, m_F \pm 1 \rangle$ has the same magnitude as an ideal electronic spin 1/2 transition $\langle m_s | S_y | m_{s'} \rangle = 0.5$. Only the ten transitions with a matrix element greater than 0.25 are shown in Fig. 2a. Characteristics for the transitions probed by our resonators are given in Extended Data Table I.

Single-spin coupling to the resonator The spin-resonator interaction is described by a Jaynes-Cummings Hamiltonian $\hbar g(a^\dagger \sigma_- + a\sigma_+)$, where a (resp. $a^\dagger$) is the field annihilation (resp. creation) operator, σ_- (resp. σ_+) the spin lowering (resp. raising) operator, and g the spin-resonator coupling strength. For the Bi:Si transitions $|F, m_F\rangle \leftrightarrow |F + 1, m_F - 1\rangle$ probed by the resonators, g can be expressed as $g = \gamma_e \langle F, m_F | S_x | F + 1, m_F - 1 \rangle \|\delta \mathbf{B}_\perp\|$ [17], where $\delta \mathbf{B}_\perp$ is the component of the resonator field vacuum fluctuations orthogonal to $\mathbf{B_0}$. Considering the orientations for $\mathbf{B_0}$ and $\delta \mathbf{B}$ shown in Fig. 1b, we get:

$$g(\theta) = \gamma_e \langle F, m_F | S_x | F + 1, m_F - 1 \rangle \sqrt{\delta B_y^2 \cos(\theta)^2 + \delta B_z^2} \tag{2}$$

To estimate the coupling constant distribution $g(0)$ for a given transition, one needs to estimate the vacuum field fluctuations $\delta \mathbf{B}$ in the spin ensemble region. This is obtained using COMSOL software and assuming a non-homogeneous current density distribution in the superconducting aluminium wire [32]. The total current flowing through the wire cross-section is given by $\delta i = \omega_0 \sqrt{\hbar/2Z_0}$, $Z_0 = \sqrt{L/C}$ being the resonator impedance, determined to be $44\,\Omega$ via electromagnetic simulations realised in CST Microwave Studio. In all the work presented in the main text, the measurements were done on the low-field peak of transition $|F, m_F\rangle = |4, -4\rangle \leftrightarrow |5, -5\rangle$, which has been attributed to spins residing

under the wire. From the spin implantation profile (see Fig 1b) and the microwave field $\delta\mathbf{B}$ spatial dependence restrained to the area under the wire ($|y| < 2.5\,\mu\text{m}$), the relevant coupling constant distribution can be extracted. This yields a very asymmetric coupling distribution sharply peaked around $g/2\pi = 56\,\text{Hz}$ with a 2-Hz width at half maximum for the transition $|4, -4\rangle \leftrightarrow |5, -5\rangle$ with $\theta = 0$. A more detailed derivation of the coupling constant and its estimate at angle $\theta = 0°$ is available in [17].

Average intra-cavity photon number $\bar{\text{n}}$. The average intra-cavity photon number $\bar{n}$ of a pulse of power P_{in} at the cavity input is evaluated by $\bar{n} = \frac{4\kappa_1 P_{\text{in}}}{\hbar\omega_0(\kappa_1+\kappa_2+\kappa_L)^2}$, κ_1 and κ_2 being the couplings to the input and output antennas and κ_L the resonator internal losses. From a previous calibration of the experimental setup[17] we estimate that we can determine P_{in} with an accuracy of $\approx 1\,\text{dB}$. The values of κ_1, κ_2 and κ_L are determined experimentally by measuring each element of the resonator scattering matrix and fitting to the well-known input-output formulae [33], see Extended Data Table II.

Data acquisition and echo signal The full description of the experimental setup is available in [17]. The use of a Josephson Parametric Amplifier allows us to reach a quantum-limited sensitivity. In addition to the Hahn-echo sequence, we use a Carr-Purcell-Meiboom-Gill sequence[34] for every echo acquisition. For all A_Q data points presented in this work, 10 π pulses are added after the first echo to recover 10 extra echoes, that are subsequently averaged to boost the signal to noise ratio. This scheme allows us to acquire data in single-shot readout. Each A_Q data point is a single-shot measurement, the error bars are determined by the variance of a pool counting at least $n = 200$ measurements, taken in similar conditions.

Experimental determination of T_1 at resonance The inversion-recovery sequence is used to measure the spin relaxation time T_1, see Fig. 2d. Spin polarisation is measured with the following Hahn echo sequence: 50-μs-long $\pi/2$ pulse, delay $\tau = 500\,\mu\text{s}$, and 100-μs-long π pulse). The pulse durations were chosen such that only spins within a narrow spectral range were detected, producing a well-defined Purcell-limited T_1. Indeed, since the probed ensemble of spins has a larger linewidth $\Delta\omega = 2\,\text{MHz}$ than our resonators, the signal emitted during the spin-echo comes from a subset of the ensemble of spins, with a frequency spectrum at least as large as the resonator bandwidth. Spins probed at the edges of the bandwidth of the resonator will have longer Purcell relaxation times: for instance those detuned by $\delta = \kappa$ have an expected Purcell relaxation time five times slower than the T_1

time expected at perfect resonance, see Extended Data Figure 1a. The contribution of those spins with a longer decay time to the signal will result in an averaging effect, meaning that the measured T_1 will be erroneously longer than predicted.

In order to suppress this effect, we reduce the bandwidth of the readout sequence so as to collect signal only from spins very close to the resonance. The response function of a pulse of length t_p incident on a cavity with bandwidth κ at frequency ω_0 is expressed as :

$$\mathcal{R}(\omega) = [2\sin c(t_p(\omega - \omega_0)/2)]^2 \times \mathcal{R}_{cav}(\omega) = [2\sin c(t_p(\omega - \omega_0)/2)]^2 \times \frac{1}{1 + 4\left(\frac{\omega - \omega_0}{\kappa}\right)^2}$$

As shown on Extended Data Figure 1a, for the narrowest bandwidth $\kappa/2\pi = 23\,\text{kHz}$ of resonator A, pulses of $5\,\mu\text{s}$ are heavily filtered by the resonator and have the same bandwidth whereas $100\,\mu\text{s}$-long pulses have a reduced bandwidth of $\approx 10\,\text{kHz}$. In case of $100\,\mu\text{s}$-long excitation pulses, the Rabi frequency is such that only spins with $|\delta|/2\pi \leq 5\,\text{kHz}$ will contribute to the signal. This corresponds to a dispersion of only 5% for the expected Purcell relaxation times, which is negligible. To illustrate the averaging effect, two inversion recovery curves are shown on Extended Data Figure 1b with readout pulses of $5\,\mu\text{s}$ and $100\,\mu\text{s}$. The former yields $T_1 = 0.65\,\text{s}$, which is a factor 2 higher than predicted by the Purcell effect whereas the lattest yields the expected value $T_1 = 0.35\,\text{s}$.

Thus Figure 2d shows an inversion recovery sequence that has a readout echo sequence with a narrow bandwidth ($t_\pi = 100\,\mu\text{s}$, $t_{\pi/2} = t_\pi/2$) to suppress contribution from spins with a lower decay rate, and an inversion pulse with large-bandwidth ($t_\pi = 5\,\mu\text{s}$) in order to maximize the efficiency of the inversion.

The spin energy relaxation time T_1 being of order $1\,\text{s}$, we choose a repetition rate γ_{rep} sufficiently low to allow full relaxation of the spins in-between successive inversion recovery sequences, $\gamma_{\text{rep}} = 0.04\,\text{Hz}$.

Experimental determination of spin-cavity detuning dependent relaxation rates The spins are detuned from the cavity by applying an additional bias pulse on one of the Helmholtz coils used to apply the static field $\mathbf{B_0}$. The extra bias pulse is output by a pulse generator with $50\,\Omega$ output impedance placed in parallel to the DC supply of one of the Helmholtz coils. To minimize the effect of transients due to the $1\,\text{Hz}$ bandwidth of the coils, buffer times of $1\,\text{s}$ are added after ramping the coil up and down. To limit the loss of signal during those buffer times, we use an angle $\theta = 45°$ and work with resonator B in order to have a longer $T_1(0) = 1.68\,\text{s}$. Applying a magnetic field pulse to a single

coil instead of both coils deviates θ by $4°$ at most. The value of $T_1(0)$ was measured with inversion recovery. All the data presented in Fig. 3 and in Extended Data Figure 2 were done in a separate run. The quality factor of resonator B dropped from $Q = 1.07 \times 10^5$ to $Q = 8.9 \times 10^4$ due to slightly higher losses, yielding the resonator bandwidth $\kappa/2\pi = 82\,\text{kHz}$.

To observe the long relaxation times, such as those measured in Fig. 3, inversion recovery is not an ideal method. Indeed, when the spin linewidth is broader ($\sim \times 20$) than the excitation bandwidth and when the thermalization time is very long, one can observe polarization mixing mechanisms [35, 36], spectral and spatial spin diffusion being the most relevant to our case, as the system is only constituted from one species. If one tries to measure the relaxation from spins that have been detuned by an amount $\delta/2\pi = (\omega_s - \omega_0)/2\pi = 3.8\,\text{MHz}$ during a lapse of time T with an inversion recovery sequence (Extended Data Figure 2a), one observes a double exponential relaxation (Extended Data Figure 2d, green), pointing towards the existence of a spin diffusion mechanism.

Spin diffusion is prevented by suppressing any polarization gradient along the spin line, which leads us to use a saturation recovery scheme instead of inversion recovery. The simplest saturation recovery scheme (Extended Data Figure 2b) consists of sending a strong microwave tone resulting in the saturation of the line, producing an incoherent mixed state with the population evenly shared between excited and ground states. Nevertheless, a relaxation time measured with this scheme still yields a double-exponential decay (Extended Data Figure 2d, orange), with time constants similar to the inversion recovery case. This implies that the saturation of the line is insufficient.

To improve the saturation, one can sweep the magnetic field during the saturation pulse so as to bring different subsets of the spin line to resonance and realize a full saturation. The adopted sweep scheme is shown on Extended Data Figure 2c. The corresponding relaxation curve fits well to a simple exponential decay (Extended Data Figure 2d, blue), indicating the suppression of the spin diffusion effect.

One can further check the quality of the saturation by measuring the polarization across the full spin linewidth immediately after saturation. To realize such scans (Extended Data Figure 2e), we apply the relevant saturation pulse at ω_0, then apply a magnetic field pulse $B_\delta = (\omega_s - \omega_0)/\gamma_e$ and measure the echo signal $A_Q(\omega_s)$ with a Hahn echo sequence. When no saturation pulse is applied, the measured echo signal $A_{Q0}(\omega_s)$ is a measure of the full polarization $-\langle S_z(\omega_s) \rangle = +1$ (black curve) and shows the natural spin linewidth. When studying

19

an excitation pulse, the polarization of the spins is given by $-\langle S_z(\omega_s)\rangle = A_Q(\omega_s)/A_{Q0}(\omega_s)$, where $A_Q(\omega_s)$ is the measured echo signal. Thus $-\langle S_z(\omega_s)\rangle = -1$ indicates full inversion, $\langle S_z(\omega_s)\rangle = 0$ saturation and $-\langle S_z(\omega_s)\rangle = +1$ return to thermal equilibrium. The green, orange and blue curves are taken after respectively a π pulse **a)** and a saturation without field sweep (**b**) and with field sweep **c)**. At resonance, one expects a change of S_z from -1 to +1 for a π pulse and from -1 to 0 for a saturation pulse. Due to the coil transient time, all three curves shows a partial relaxation. If the saturation was optimal and no partial relaxation was occurring, one should observe $S_z = 0$ for any detuning δ. Among the two saturations **b)** and **c)** studied here, only the last saturation scheme **c)** equally saturates the line. The basic saturation **b)** has a bandwidth $\approx 250\,\text{kHz}$ and the π pulse **a)** bandwidth is similar to the cavity $\kappa/2\pi = 82\,\text{kHz}$. This confirms that only in scheme **c)** can spin diffusion be fully suppressed and yield a simple exponential decay relaxation. This is this last scheme that is used to measure the 22 relaxation rates at different detunings δ of Fig.4.

The global fit shown on Fig. 4c it is obtained by using equation $T_1(\delta)^{-1} = \Gamma_{\text{P}} + \Gamma_{\text{NR}}$ which may be expressed as $T_1(0)^{-1}\left(1 + 4\left(\frac{\delta}{\kappa}\right)^2\right)^{-1} + \Gamma_{\text{NR}}$ to involve only experimentally determined parameters. Indeed, κ is precisely determined by measuring the quality factor of the resonator at low power while $T_1(0)$ is determined by an inversion recovery sequence as mentioned above. δ has been determined via precise calibration of the coil pulse, thus the only remaining free parameter in the fit is Γ_{NR}, yielding $\Gamma_{NR}^{-1} = 1600\,\text{s}$. The errors bars come from the accuracy of the relaxation rates fits.

Practical considerations for the application of cavity-induced relaxation in magnetic resonance The experiments described in the main text take place at low magnetic field ($B_0 < 10\,\text{mT}$) and low temperature ($T \approx 20\,\text{mK}$) using a dilution refrigerator, which are unusual conditions for magnetic resonance measurements . However, as we discuss below, with straightforward modifications, cavity-induced relaxation could be observed in other environments, broadening the class of spin systems which could be used.

Indeed, superconducting micro-resonators can withstand large magnetic fields (up to $\approx 1\,\text{T}$) while keeping a large quality factor ($Q_i \sim 2 \times 10^5$) [37–39] if they are patterned in metals such as Nb, NbN, or NbTiN, instead of Al, as we have used. This would enable applying our results to a much larger class of spin systems, including typical electron spins with $g \approx 2$. Similar observations can be made for temperature: Nb, NbN, and NbTiN have a higher critical temperature than Al, which would permit the use of temperatures of

1-4K (accessible with conventional liquid helium cryostats). Note however that temperature plays other important roles, beyond helping to maintain a small κ, because the Purcell effect brings spins into thermal equilibrium with the cavity field. For example, at the microwave frequencies used in our experiments (7.3 GHz), temperatures below 70 mK are required for a spin polarization $> 99\%$. Higher temperatures could be used at a cost in the degree of spin polarization, but this could be addressed by moving to higher frequencies. A third factor when considering the operating temperature is that cavity-induced relaxation can only be exploited where it out-competes intrinsic processes such as spin-lattice relaxation — for most spin systems this translates into temperatures around liquid helium temperatures.

The possibility of cavity-induced relaxation with conventional electron spin systems might suggest other applications, beyond using a faster return to thermal equilibrium to increase signal averaging rates. In particular, we consider the possibility of cavity-assisted Dynamic Nuclear Polarization (DNP), either via the so-called Solid Effect (SE) or via the Overhauser Effect (OE) which was recently observed in solids [40]. In the SE, a nuclear spin of frequency ω_n coupled to an electron spin of frequency ω_e sees its equilibrium polarization enhanced by irradiating it with microwaves at $\omega_e + \omega_n$, provided the electron spins return quickly enough to equilibrium. Tuning a cavity on resonance with the electron spin transition at ω_e could provide an alternative relaxation mechanism to phonons, thus avoiding for instance phonon bottleneck effects and/or relieving the need to apply large magnetic fields. In the OE, saturating the spin transition by applying microwaves at ω_s enhances the nuclear spin polarization because of the existence of electron-nuclear spin cross-relaxation processes, which could be enhanced by tuning a cavity at $\omega_e - \omega_n$.

---

[31] Gary Wolfowicz, Alexei M Tyryshkin, Richard E George, Helge Riemann, Nikolai V Abrosimov, Peter Becker, Hans-Joachim Pohl, Mike LW Thewalt, Stephen A Lyon, and John J L Morton, "Atomic clock transitions in silicon-based spin qubits," Nature Nanotechnology **8**, 561–564 (2013).

[32] T. Van Duzer and C. Turner, *Superconductive Devices and Circuits* (Prentice Hall PTR, 1999).

[33] A. Palacios-Laloy, *Superconducting qubit in a resonator : test of the Leggett-Garg inequality and single-shot readout* (2010).

[34] F Mentink-Vigier, A Collauto, A Feintuch, I Kaminker, V Tarle, and D Goldfarb, "Increasing sensitivity of pulse epr experiments using echo train detection schemes," Journal of Magnetic Resonance **236**, 117–125 (2013).

[35] N. Bloembergen, "On the interaction of nuclear spins in a crystalline lattice," Physica **15**, 386–426 (1949).

[36] A. Abragam, *Principles of Nuclear Magnetism* (Oxford Science Publications, Clarendon Press, 1986).

[37] S. E. de Graaf, D. Davidovikj, A. Adamyan, S. E. Kubatkin, and A. V. Danilov, "Galvanically split superconducting microwave resonators for introducing internal voltage bias," Applied Physics Letters **104**, 052601 (2014), http://dx.doi.org/10.1063/1.4863681.

[38] I. Wisby, S. E. de Graaf, R. Gwilliam, A. Adamyan, S. E. Kubatkin, P. J. Meeson, A. Ya. Tzalenchuk, and T. Lindstrm, "Coupling of a locally implanted rare-earth ion ensemble to a superconducting micro-resonator," Applied Physics Letters **105**, 102601 (2014), http://dx.doi.org/10.1063/1.4894455.

[39] N. Samkharadze, A. Bruno, P. Scarlino, G. Zheng, D. P. DiVincenzo, L. DiCarlo, and L. M. K. Vandersypen, "High Kinetic Inductance Superconducting Nanowire Resonators for Circuit QED in a Magnetic Field," ArXiv e-prints (2015), arXiv:1511.01760 [cond-mat.mes-hall].

[40] T. V. Can, M. A. Caporini, F. Mentink-Vigier, B. Corzilius, J. J. Walish, M. Rosay, W. E. Maas, M. Baldus, S. Vega, T. M. Swager, and R. G. Griffin, "Overhauser effects in insulating solids," The Journal of Chemical Physics **141**, 064202 (2014), http://dx.doi.org/10.1063/1.4891866.
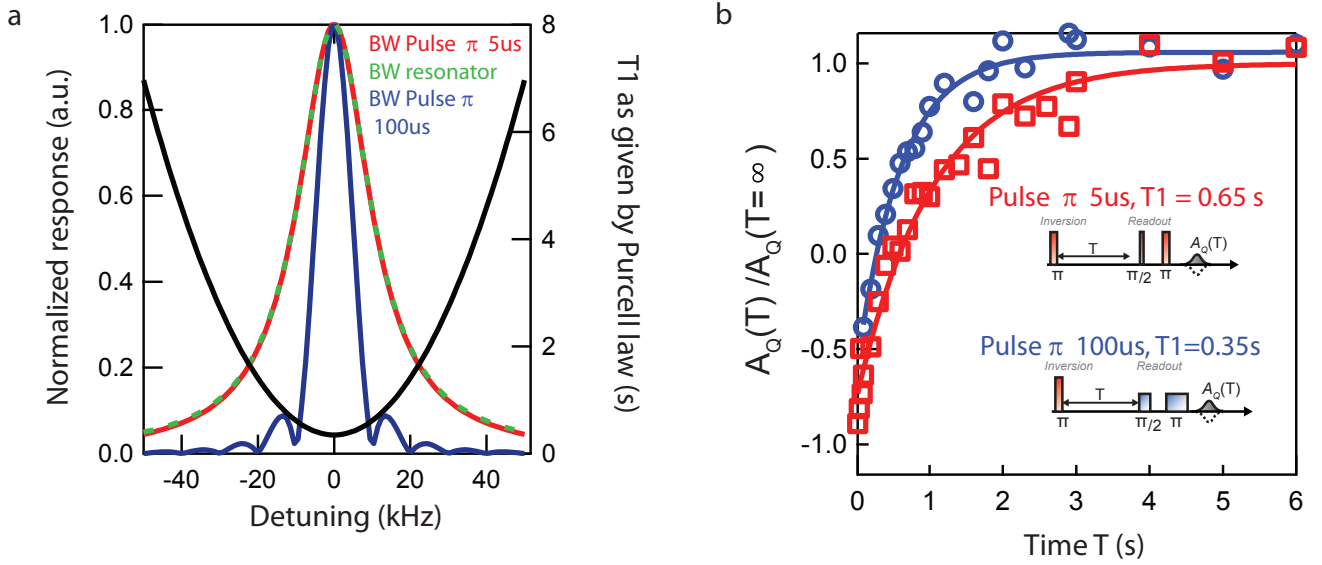
EXTENDED DATA

Transition	df/dB	$\langle F, m_F | S_x | F+1, m_F - 1 \rangle$
$|4, -4\rangle \leftrightarrow |5, -5\rangle$	$-25.1\,\text{GHz/T}$	0.47
$|4, -3\rangle \leftrightarrow |5, -4\rangle$	$-19.2\,\text{GHz/T}$	0.42
$|4, -2\rangle \leftrightarrow |5, -3\rangle$	$-13.5\,\text{GHz/T}$	0.37

Extended Data Table I. Relevant Bi:Si transitions and their characteristics.

Resonator	$\omega_r/2\pi$	Q	κ_1 (s^{-1})	κ_2 (s^{-1})	κ_L (s^{-1})
A	7.2467 GHz	3.2×10^5	1.3×10^4	5.8×10^4	7.5×10^4
B	7.3054 GHz	1.1×10^5	3.6×10^4	3.1×10^5	8.2×10^4

Extended Data Table II. Resonator characteristics.

Extended Data Figure 1. Excitation pulse bandwidth effect on T_1 measurement. **a)** Computed pulse bandwidth, respectively for a 5(100)-μs π pulse, in red (blue) incident on a cavity with $\kappa/2\pi = 23\,\text{kHz}$ (green dashes). To illustrate the averaging effect of the pulse bandwidth on T_1 measurements, the expected Purcell T_1 curve (black line) as a function of spin-cavity detuning is plotted on the right scale, with $T_1(0) = 0.35\,\text{s}$ and $\kappa/2\pi = 23\,\text{kHz}$. **b)** T_1 measurements for two different π pulse lengths, measured on resonance with resonator A. $\pi = 100\,\mu\text{s}$ (red) yields $T_1 = 0.35\,\text{s}$, which is in agreement with the Purcell rate . $\pi = 5\,\mu\text{s}$ (red) yields $T_1 = 0.65\,\text{s}$, a factor 2 away from the accurate value.

25
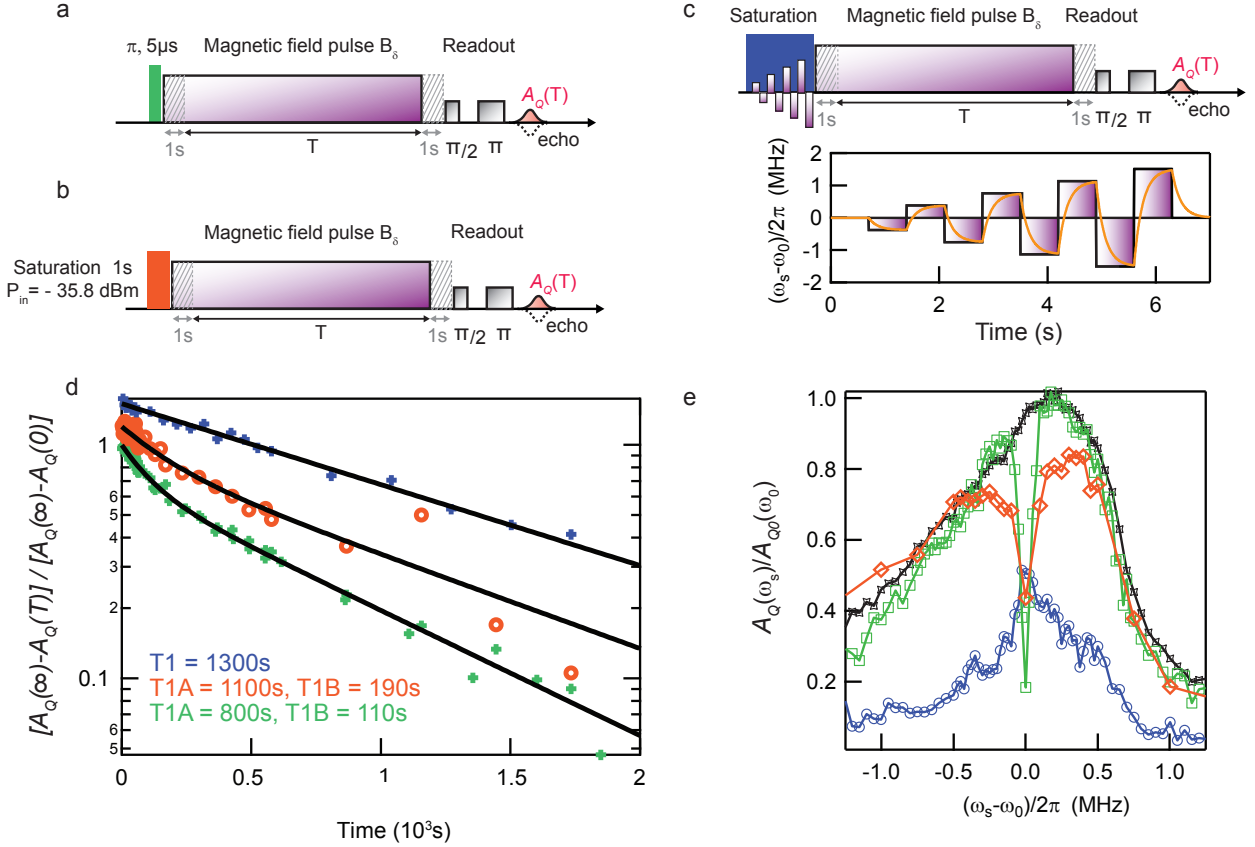
Extended Data Figure 2. Spectral spin diffusion. **a-c)** T_1 measurement sequence when spins are detuned from the cavity by applying a magnetic field B_δ, providing a detuning $\delta = \omega_s - \omega_0 = 2\pi\gamma_{\text{eff}}B_\delta$, with $\gamma_{\text{eff}} = df/dB(B_0)$. **a)** uses a $\pi = 5\,\mu s$ pulse to realise a so-called inversion recovery sequence, **b)** and **c)** are saturation recovery sequences: **b)** uses a 1-s-long strong microwave pulse sent at cavity resonance whereas **c)** has in addition a magnetic field scan shown on the bottom part. Depicted in orange is the expected magnetic field profile due to the the coil filtering, assuming the coil to be an order-1 low-pass filter of bandwidth 1-Hz. **d)** T_1 measurements for sequence **a)** (green), **b)** (orange), **c)** (blue) for $\delta/2\pi = 3.8\,\text{MHz}$. Fits (black lines): **a)** & **b)** have a double exponential decay whereas **c)** is a simple exponential. We attribute this double-exponential decay to spin diffusion. **e)** Spectral profiles of excitation pulses **a)** (green), **b)** (orange) & **c)** (blue). The sequence is as follows: send the excitation pulse, detune the spins and measure $A_Q(\omega_s)$. Black line is the reference profile without any excitation pulse, yielding reference $\langle S_z(\omega_s)\rangle = -A_{Q0}(\omega_s)/A_{Q0}(\omega_s)$. When an excitation pulse is sent, one can access $\langle S_z(\omega_s)\rangle = -A_Q(\omega_s)/A_{Q0}(\omega_s)$. Note that neither the π profile or the saturation profile reach either the full inversion $+1$ or full saturation 0 at resonance. This is an artefact due to the coil transient time.